## ResearchOnline@JCU



This is the author-created version of the following work:

Prajapati, Megha, Ravi Kant, Chhaya, Allende, Scarlett, and Jacob, Mohan V. (2023) Metal organic framework derived NiCo layered double hydroxide anode aggregated with biomass derived reduced graphene oxide cathode: A hybrid device configuration for supercapattery applications. Journal of Energy Storage, 73.

Access to this file is available from:

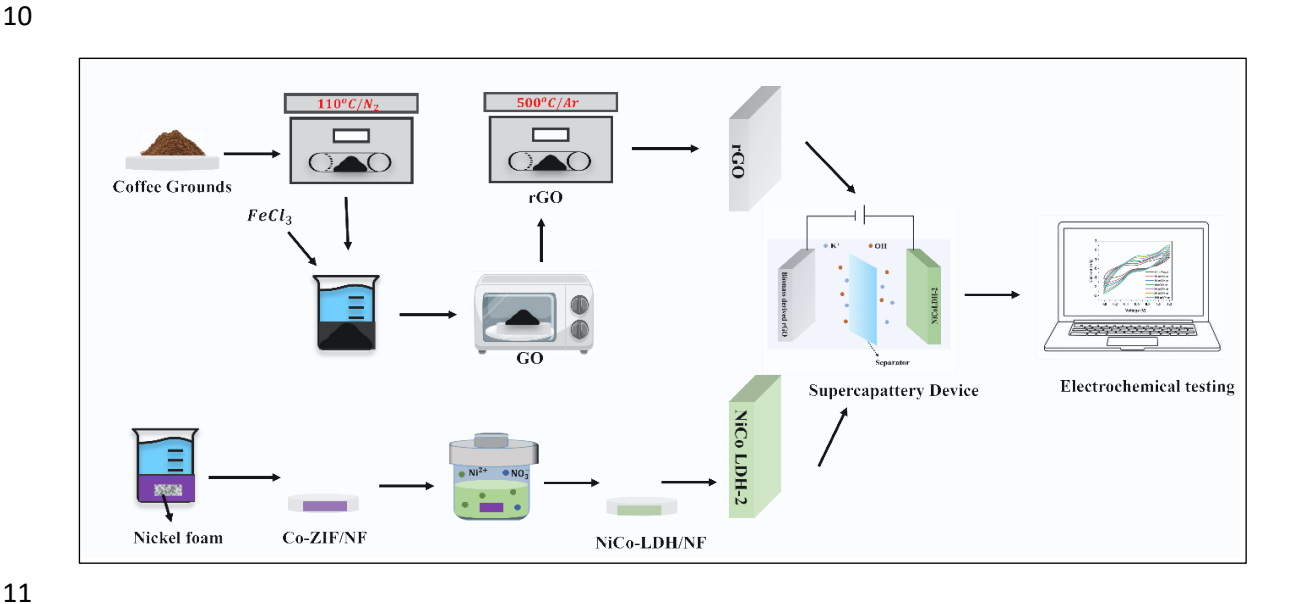
https://researchonline.jcu.edu.au/80805/

© 2023 Elsevier Ltd. All rights reserved.

Please refer to the original source for the final version of this work:

https://doi.org/10.1016/j.est.2023.109264

- 1 Metal Organic Framework derived NiCo Layered Double Hydroxide anode
- 2 aggregated with biomass derived reduced Graphene oxide cathode: A
- 3 hybrid device configuration for supercapattery applications
- 4 Megha Prajapati<sup>1,2</sup>, Chhaya Ravi Kant<sup>1\*</sup>, Scarlett Allende<sup>2</sup>, Mohan V. Jacob<sup>2</sup>
- <sup>1</sup>Department of Applied Sciences and Humanities, Indira Gandhi Delhi Technical University
- 6 for Women, Delhi-110006, INDIA
- <sup>2</sup>Electronics Materials Lab, College of Science and Engineering, James Cook University,
- 8 Townsville, QLD 4811, Australia
- 9 Corresponding Author E-mail \*chhayaravikant@igdtuw.ac.in



#### **Graphical Abstract**

Abstract

12

13

14

15

16

17

18

19

20

21

22

Metal-organic frameworks (MOFs), due to its exceptional characteristics like high specific surface area and design diversity, serve as an outstanding sacrificial template in forming layered double hydroxides (LDHs) for highly efficient electrodes in supercapattery devices. In this work, we have prepared bimetallic layered Nickel Cobalt LDH via in-situ etching of Co-ZIF, in different Nickel concentrations directly on Ni foam that enhances the interfacial contact between substrate and the material. The optimised NiCo LDH-2 sample exhibited remarkable electrochemical behaviour with fast electrolyte ion diffusion kinetics ideal for supercapattery device and delivered a high specific capacitance of 2567 Fg<sup>-1</sup> at 1 Ag<sup>-1</sup>. Further, the

- 1 supercapattery device assembled with Ni-Co LDH as anode and rGO derived from a
- 2 sustainable source as cathode demonstrated an energy density of 21 Whkg<sup>-1</sup>, power density of
- 3 0.307 kWkg<sup>-1</sup> and good cyclic stability with capacitance retention of 88.89 % along with
- 4 coulombic efficiency of 90.58 % over 1500 cycles. This work proposes an effective approach
- 5 for designing layered NiCo-LDH that can be further extended to the synthesis of other
- 6 transition metal-derived LDH for supercapattery devices.
- 7 **Keywords:** Supercapattery; Metal-Organic Frameworks; Energy density; Power density

10

25

#### 1. Introduction

Constant growth of new portable electronic technologies and a modernized lifestyle has 11 increased the demand for advanced energy storage devices. To address these challenges, 12 13 intensive research on electrochemical energy storage (EES) devices comprising batteries [1]-[4], supercapacitors (SCs) [5]–[8] and supercapatteries [9]–[11] has been greatly considered 14 over the past few decades. In this aspect, batteries, which include materials like metal oxides, 15 hydroxides, phosphates, and sulphides that facilitate faradaic processes for charge storage 16 mechanism offer tremendous energy density but attribute poor power density and a quickly 17 diminishing cyclability. On the other hand, SCs have been classified into two groups depending 18 on their charge storage mechanism: electrical double-layered capacitors (EDLCs) [12], [13] 19 sand pseudocapacitors. The mechanism of non-faradaically adsorbing-desorbing electrolyte 20 ions is accountable for charge storage processes in EDLCs, that primarily use carbonaceous 21 materials (activated carbon, rGO, CNTs, etc.). Whereas, transition metal oxides/hydroxides 22 phosphides/sulphides/halides [14]–[18] and conducting polymers are predominantly utilized in 23 24 pseudocapacitors in which the surface redox reaction is responsible for the charge storage

mechanism. SCs' offer primary benefits like extended cycle life, high power densities, quick

charge-discharge times, and environmentally friendly behaviour [17]. But their low energy 1 density is still a challenge posing a major hindrance in large-scale commercialization. It is 2 evident that both technologies, despite their merits do have their drawbacks which indicate that taken alone, none of them can meet the enormous energy demand of this world. The development of hybrid electrochemical energy storage technologies that combine the use of batteries and capacitive-type materials in a single device is a significant step towards 7 addressing the aforementioned drawbacks [20], [21]. Due to the addition of carbonaceous material of EDLCs as a negative electrode and MOF-derived LDH as a positive electrode, the device shows increased energy density while maintaining power density with high cyclability. Not only the active material, the method utilized in the fabrication of electrodes and also their surface interaction with electrolytes have a major impact on the overall performance of the device. Therefore, the utmost importance is to design electrode materials that possess high kinetic and electrochemical activity. LDHs with unique 2D hydrotalcite-like structures are regarded as exceptional electrode material in energy storage systems because of their relatively high specific surface area and redox activities with tuneable chemical compositions, and the ability for rapid intercalation/deintercalation of charged ions. The formula for LDHs that are generally used is  $[M_x^{3+}M_{1-x}^{2+} (OH)_2]^{x+} [N_{x/n}^{n-}]^{x-}$ , where,  $M^{3+}$  (Co, Ni, Mg, and Zn), and  $M^{2+}$ (Cr, Al, Ga, and V) are the trivalent and divalent metal cations in octahedral sites in brucitelike layers, and N<sup>n</sup>- (NO<sub>3</sub><sup>-</sup>, CO<sub>3</sub><sup>-</sup> and water molecules) are anions placed in the interlayer space of LDH. The laminar LDH structures and flexible anionic exchange characteristics facilitated electron and ion flow throughout the charging and discharging process, not only at the surface but also in the entire crystalline nanostructure of LDH, enabling it to act as a battery-like electrode material. Despite advancements, low mechanical strength, poor electrical conductivity, and severe agglomeration of LDH electrode materials preclude it from achieving high theoretical efficiency [22], [23]. Hence, in order to achieve outstanding performance for

3

4

5

6

8

9

10

11

12

13

14

15

16

17

18

19

20

21

22

23

24

25

- 1 supercapattery electrodes, a simple and effective self-template technique for synthesising
- 2 LDHs with adjustable morphology is required [23].
- 3 Metal-organic frameworks (MOFs) are ordered inorganic-organic hybrid porous crystalline
- 4 materials, that have garnered a lot of attention because of their large surface area, high porosity,
- 5 and structural with functional diversity, and have been thoroughly investigated in a variety of
- 6 domains due to their adjustable metal centre, and high ordered structure. MOFs, particularly
- 7 zeolitic imidazolate framework-67 (ZIF-67), a sub-member of MOF, are proven to be an
- 8 attractive template for the preparation of various nanostructured materials, including carbon
- 9 and metal (oxides, hydroxides, phosphides, and sulphides) derived materials for
- 10 electrochemical energy storage and conversion operations because of its high porosity,
- tuneable shape, and exceptional chemical robustness [24]–[27].
- 12 In recent years, ZIF-derived LDHs have gained an immense interest in energy storage
- operations. Furthermore, in-situ growth of these nanostructures over a flexible substrate such
- as nickel foam, carbon cloth, etc. tends to avoid the agglomeration of LDH nanoarray that
- extends their participation in the energy conversion and storage (ECS) system, significantly
- improving the utilization of electroactive materials. Wang et al. [28] reported in-situ grown
- 17 NiCo-LDH on carbon cloth using a controlled hydrolysis technique and achieved a high
- specific capacitance of 2242.9 Fg<sup>-1</sup> [28]. Tahir et al. [22] have obtained the bimetallic CoNi-
- 19 LDH nanosheets using ZIF precursor that exhibited specific capacitance (1877 Fg<sup>-1</sup> at 1 Ag<sup>-1</sup>)
- 20 [22]. Even though these bi-metallic layered hydroxides have improved electrochemical
- 21 performance, it remains a challenge to increase the active sites and interacting surfaces to
- 22 further improve the materials' electrochemical parameters. As a result, the template-directed
- 23 technique is effective and has garnered much interest among LDH synthesis techniques.

In this study, instead of synthesizing bimetallic LDH by incorporating Co<sup>2+</sup> and Ni<sup>2+</sup> 1 simultaneously, we have grown ZIF-67 in situ on Ni foam (NF) and subsequently incorporated 2 Ni ions to synthesize NiCo LDH. By using appropriate characterisation techniques, the 3 morphological, structural, and electrochemical characteristics of NiCo-LDHs were examined. 4 The controlled concentration of Ni ion helped in growth of honeycomb-like layered sheets on 5 NF with robust adhesion. Moreover, LDH's synergistic properties lead to remarkable 6 7 electrochemical performance because of its rapid electrolyte diffusion kinetics, enhanced electroactive sites, and abundant redox active sites in electrolyte solution of potassium 8 9 hydroxide(KOH) [29]. Furthermore, the surface of hollow NiCo-LDH has numerous tiny nanosized alleys, which maximises the percolation of ions to the electrode surface, significantly 10 reducing ion transportation resistance and thereby increasing the reaction kinetics. 11 Furthermore, a novel supercapattery device has been designed with ZIF-derived LDH as 12 battery-type electrode and bio-derived rGO as an EDLCs electrode with an electrolytic solution 13 of 1 M KOH. A green, eco-friendly approach has been used to synthesize rGO from coffee 14 15 grounds using microwave pyrolysis technique. As expected, the supercapattery device can reach an energy density of 21 Whkg<sup>-1</sup> with power density of 0.307 kWkg<sup>-1</sup>, as well as good 16 cyclability with capacitance retention of 88.89 % along with coulombic efficiency of 90.58 % 17 over 1500 charge-discharge cycles. 18

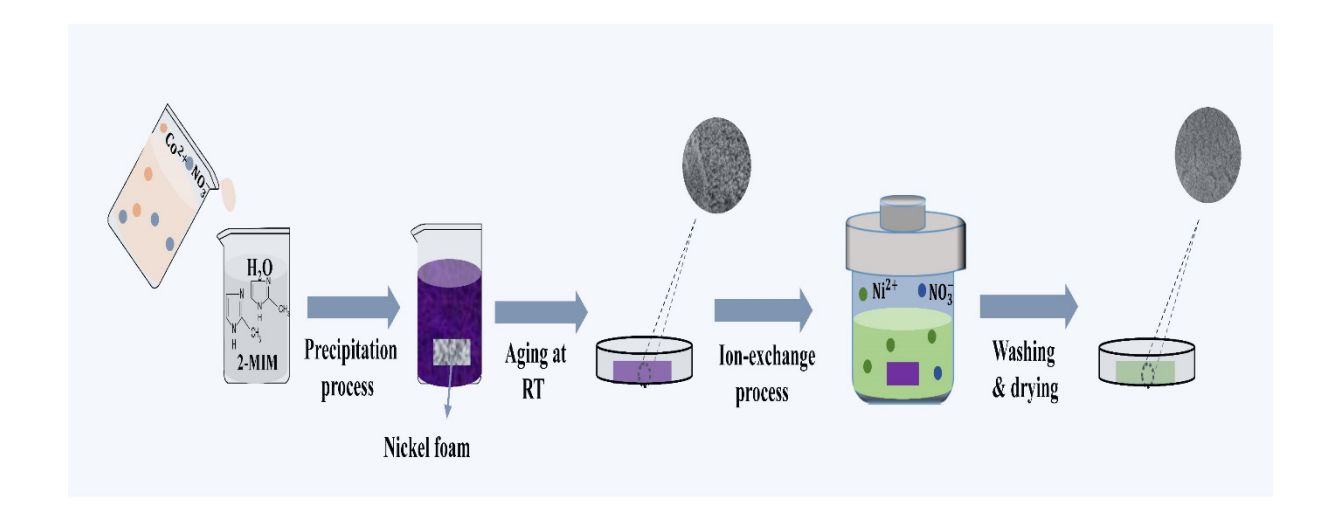
### 2. Experimental Section

20 *2.1. Materials* 

19

- Ni Foam (NF) was purchased from Nanoshel, India. 2-methylimidazole (2-MIM) (C<sub>4</sub>H<sub>6</sub>N<sub>2</sub>, AR
- 22 99%), cobalt nitrate hexahydrate (Co(NO<sub>3</sub>)<sub>2</sub>.6H<sub>2</sub>O, AR 99%), nickel nitrate hexahydrate
- 23 (Ni(NO<sub>3</sub>)<sub>2</sub>.6H<sub>2</sub>O, AR 99 %), ethanol (CH<sub>3</sub>CH<sub>2</sub>OH, AR 99%), N-methyl-2-pyrrolidone (NMP
- AR 99%), and other reagents were purchased from SRL. Potassium hydroxide (KOH, AR
- 99%), and polyvinylidene fluoride (PVDF, AR 99%) were purchased from Sigma-Aldrich. All

- the chemical reagents were of analytically pure grade and used without further purification.
- 2 2.2. Material Preparation and Methods
- 3 2.2.1. Preparation of Co-ZIF/NF
- 4 Ni foam was cleaned by acetone, ethanol and di-water under sonication for 10 minutes. In a
- 5 typical process, 40 mL aqueous Co(NO<sub>3</sub>)<sub>2</sub>.6H<sub>2</sub>O solution (25 mM) was added into a 40 mL
- 6 aqueous solution of 2-MIM (0.4 M). After stirring for 2-5 mins at 150 rpm, the cleaned nickel
- foam  $(1 \times 1.5 \text{ cm}^2)$  was immersed into the above solution and aged overnight under ambient
- 8 temperature. The prepared purple-coloured sample was taken out and washed in ethanol and
- 9 di-water several times and then dried at 60°C for 10 hours. The mass load on the sample was
- 10 about  $3 \pm 0.2 \text{ mg/cm}^2$ .
- 11 2.2.2. Preparation of Co-ZIF derived NiCo-LDH/NF
- The as-obtained Co-ZIF/NF was immersed into a 50 ml Teflon liner autoclave containing 30
- mL ethanol and 0.32 mM of Ni(NO<sub>3</sub>)<sub>2</sub>.6H<sub>2</sub>O. The autoclave was sealed and heated at 90° C for
- 14 60 mins in a hot air oven. The as-prepared silvery white coloured sample was taken out and
- washed in EtOH and DI water and then dried at 60°C overnight and the colour was found to
- change to pastel green. For comparison, different concentrations of Ni(NO<sub>3</sub>)<sub>2</sub>.6H<sub>2</sub>O (0.16, 0.32,
- and 0.48 mM) were used and considered as NiCo LDH-1, NiCoLDH-2 and NiCo LDH-3
- respectively. The mass loading was about  $1.6 \pm 0.2$  mg/cm<sup>2</sup>.



Scheme 1: Synthesis route for NiCo LDH electrode materials preparation.

#### 2.2.3. Preparation of rGO negative electrode

Graphene oxide (GO) was obtained using coffee grounds as a precursor, iron chloride (FeCl<sub>3</sub>) as chemical post-treatment, and microwave pyrolysis as a thermal conversion process. 10g of biomass was washed with ethanol and DI water until remove the impurities. The cleaned coffee ground was dried at 110° C for one hour and then pyrolyzed at 1 kW for 30 minutes under 4 m/L nitrogen flow. The resulting biochar was chemically treated with FeCl<sub>3</sub> in a weight ratio of 1:1 at room temperature for 24 hours. After this, the material was washed multiple times with distilled water and dried in an oven at 110°C for one hour. The modified biochar was repyrolyzed at 1 kW for 30 minutes. Afterwards, 2.8 g of GO powder was reduced in the tubular furnace at 500°C for 5 hours at the rate of 10° C under an Argon atmosphere. The mass of rGO was found about 2.4 g. Next, mixed slurry of rGO powder, acetylene black, and PVDF in the ratio of 8:1:1 was prepared using N-Methyl-2-pyrrolidone (NMP) as the solvent and drop casted on the piece of cleaned NF. Finally, the electrodes were dried at 60° C for 10 hours. The mass loading was about 1.50 ± 0.2 mg/cm<sup>2</sup>.

#### 2.3. Material characterization

The morphological structure of the synthesized materials was analysed by field emission scanning electron microscopy (Nova Nano FESEM 450 by FEI). Further, inner structure

morphological analysis was done by HR-TEM (EcnaiG20 at 200 kV). X-ray diffraction 1 analysis (XRD, Bruker, D8 Discover) using Cu Kα, 3 KW radiation was used to analyse the 2 crystal structure of the synthesized products. The surface area and porosity of the material were 3 analysed by Brunauer-Emmett-Teller (BET) (Nova Touch LX2 by Quantachrome). Fourier 4 transform infrared spectroscopy (FTIR, Shimadzu, Japan) was used to determine the fingerprint 5 of the vibrational modes of the material. X-ray photoelectron spectrum (XPS) of the as-6 7 prepared sample was investigated using Thermo Fisher Scientific with micro-focused X-ray (400nm spot size, 72 W, 12000V) to determine the surface properties. 8

#### 2.4. Electrochemical measurements

Electrochemical performance of samples was estimated by electrochemical workstation 10 11 (Autolab Potentiostat, USA) in 1 M KOH electrolyte in a standard three-electrodes configuration with Ag/AgCl as reference electrode (RE), platinum wire as counter electrode 12 (CE) and as prepared samples on NF as working electrode (WE) as shown in Schematic 1. 13 Cyclic voltammetry (CV) and galvanostaticcharge-discharge (GCD) measurements were 14 analysed within the potential windows of 0-0.5 V and 0-0.4 V respectively. The results of 15 electrochemical impedance spectroscopy (EIS) were obtained in the frequency range of 0.01-16 10<sup>5</sup> Hz at open circuit potential. The specific capacity (C, Cg<sup>-1</sup>), and specific capacitance (C<sub>s</sub>, 17 Fg<sup>-1</sup>) were calculated according to the GCD plots using the following formula: 18

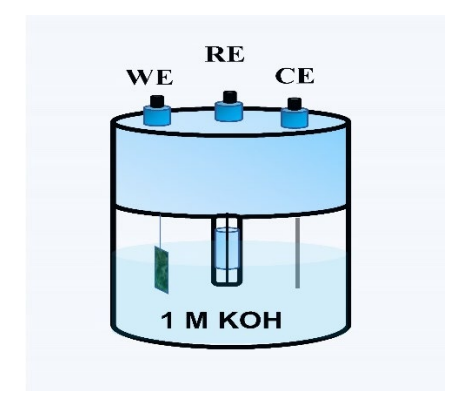
$$C = \frac{I\Delta t}{m}, C_S = \frac{I\Delta t}{m\Delta U}....(1)$$

Where, I (A) shows current density,  $\Delta t$  (sec) show discharging time, m(g) show mass of material deposited on substrate, and  $\Delta U$  (V) show the potential window.

20

21

9



2

Scheme 2: Three-electrode configuration

3

- 4 2.5. Assembly of supercapattery device
- 5 Supercapattery devices were fabricated using NiCo-LDH/NF as anode and coffee grounds-
- 6 derived rGO as cathode. The mass loading ratio of the material at each electrode was evaluated
- 7 using charge balancing rule using the following formula:

- 9 Here, m,  $\Delta U$ , and  $C_{\rm s}$  represent the mass, potential window, and specific capacitance
- 10 respectively. Where, subscript (+) (-) are for anode and cathode respectively. The specific
- capacity, power density (P, Wkg<sup>-1</sup>), and energy density (E, Whkg<sup>-1</sup>) of supercapattery were
- determined using following formulas given below:

Here,  $m_{active}$  is the active mass of both electrodes given as

3

#### 3. Result and discussion

4 3.1. Synthesis and structural characterization of NiCo LDH

5 FE-SEM image of precleaned NF (Figure 1(a)) shows a compact and smooth surface. When NF is dipped in the solution of Co(NO<sub>3</sub>)<sub>2</sub>.6H<sub>2</sub>O and 2-MIM for 7 hours, Co-ZIF is formed, seen 6 as a densely packed mesh-like structure formed with nanorods (Figure 1(b)). Co-ZIF acts as a 7 sacrificial template for the formation of NiCo-LDH using ion-exchange process, wherein 8 hydrolysis of Ni<sup>2+</sup> occurs in the presence of ethanol. H<sup>+</sup>, a byproduct of hydrolysis intrudes the 9 Co-ZIF template breaking the coordination between Co<sup>2+</sup> and 2-MIM, setting Co<sup>2+</sup> free. 10 Further, Co<sup>2+</sup> gets partly oxidised into Co<sup>3+</sup> through dissolved NO<sup>3-</sup> and O<sub>2</sub>. The Co<sup>2+</sup>/Co<sup>3+</sup> 11 coprecipitates with Ni<sup>2+</sup> to produce NiCo hydroxide layers. In a nutshell, the nanocage structure 12 13 of LDH can be attained through ethanol etching and the Kirkendall effect. Ethanol facilitates gradual dissolution of Co-ZIF template, preventing structural breakdown during hydrolysis of 14 nickel nitrate. As the Nickel nitrate solution hydrolyses in ethanol, the resulting proton 15 encourages the oxidizability of dissolved NO3- and O2 that etches the surface of Co-ZIF. This 16 leads to the oxidation of divalent cobalt to trivalent cobalt due to its low standard reduction 17 18 potential. Ultimately, LDH forms through the co-precipitation of the divalent nickel metal source and trivalent cobalt ions. The NiCo-LDH nanosheets were evenly distributed on the 19 surface of Nickel foam to form a 3D interconnected hierarchal nanonetwork. This structure is 20 21 desirable for the accessibility of active sites and also in situ growth on NF eliminates the chance of the "dead mass" making the process favourable for enhancement of capacitance with fast 22 redox reactions kinetics. 23

- 1 Amount of Ni concentration is crucial for the desired porosity of the nanostructure with
- 2 prominent morphological changes seen in Figure 1(c-e) corresponding to NiCo LDH-(1, 2, 3)
- 3 showing an interconnected, porous, 3D networked surface with formation of fine alleys.

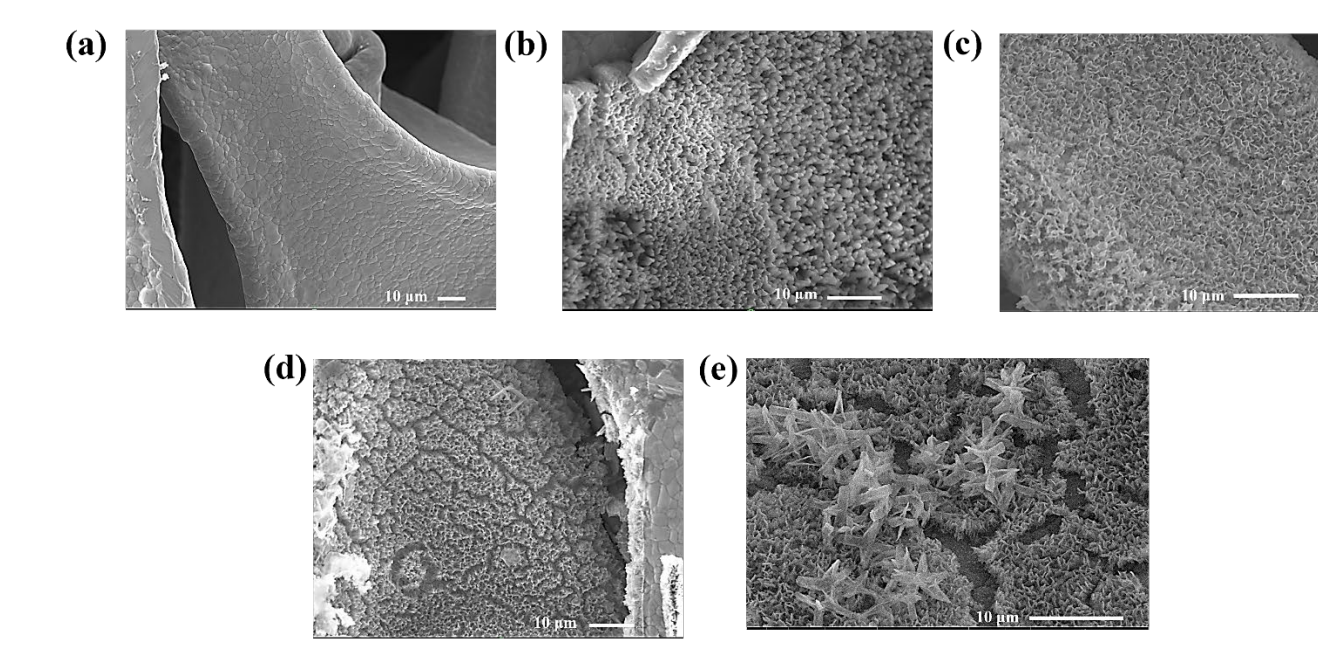


Figure 1: FE-SEM micrographs of (a) Precleaned bare Ni foam (b) Co-ZIF (c) NiCo LDH-1 (d,e)

NiCo LDH-2 (f) NiCo LDH-3 at 10µm

An increase in the Ni concentration (NiCo LDH-2) shows the alleys become deeper and wider (Figure 1(d)). This is attributed to increase in the nucleation rate between organic ligands and metal species resulting in well-defined, self-assembly of 3D hierarchical, honeycomb-like nanostructures with initiation of star-like nanostructures [30]. These alleys deliver adequate accessible active sites and diffusion pathways for fast redox reactions. The networked structure provides high electroactive surface area, and wider interspacing for electrolytic ions to penetrate improving the charge storage behaviour [31]. Further increase in Ni concentration (NiCo LDH-3) (Figure 1(e)) shows wider cracks along with an increase in the density and size of the star-like nanostructures, that cluster to constrict the pores limiting the chances of electrochemical activity. The Ni: Co ratio of 1:3.6, 1:5.4, and 1:4.2 was estimated for NiCo-

- 1 LDHs samples (1, 2 and 3 respectively) (Table S1). This confirms that Ni concentration plays
- 2 a significant role in the morphology change of the sample. At high concentration, the Co-ZIF
- 3 template dissolve too quickly to form enlarged alleys with lastly yield star like structure

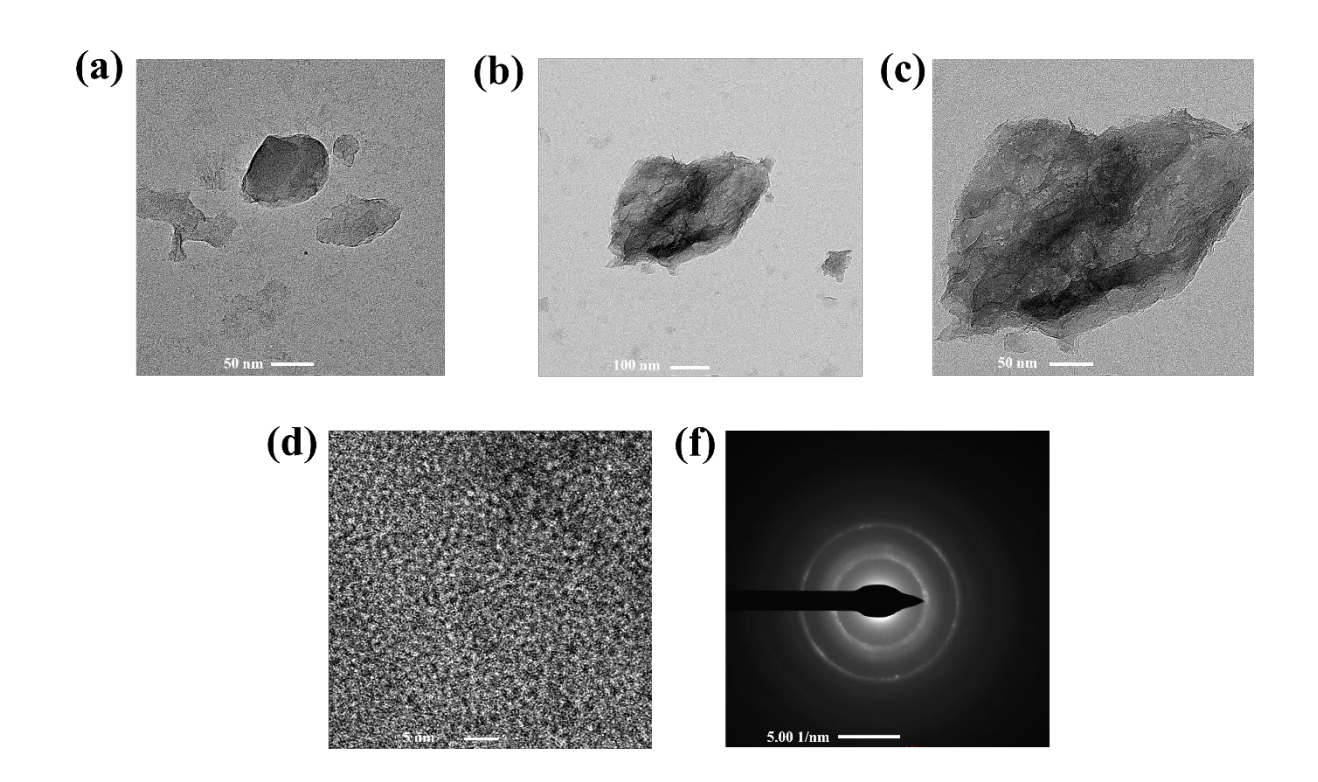


Figure 2: HR-TEM images of (a) Co-ZIF (b,c,d) NiCo LDH-2 at 100nm, 50nm and 5nm respectively (e) SAED pattern of NiCo LDH-2

The inner structure and morphology of Co-ZIF and NiCo LDH-2 structures are meticulously examined by TEM characterization. TEM images reveals that the original shape of 2D Co-ZIF is preserved (Figure 2a) even after hydrothermal reaction with nickel nitrate (Figure 2b, c, d). Furthermore, the surface morphology undergoes modification with small nanosheet-like structures intertwining to form 3D stacked structure, indicating the formation of NiCo-LDH, which aligns with the SEM results. The TEM pattern lacks distinct lattice fringes indicating the amorphous nature of NiCo-LDH sample. Figure 2d depicts the hollow and porous structure of NiCo-LDH, which promotes electrolyte transport and boosts the electrochemically active sites, thereby enhancing the electrochemical activity. The selected area electron diffraction

1 (SAED) pattern (Figure 2e) showcases diffused rings, a consequence of the sample's amorphous nature. 2 FTIR spectra of the samples are shown in Figure 3(a). The 2-MIM ligand's presence is 3 primarily responsible for the existence of Co-ZIF peaks. The peaks at 746, 1139, and 1417 cm<sup>-1</sup> 4 <sup>1</sup> are ascribed to stretching and bending modes of the imidazole ring, while peak at 1635 cm<sup>-1</sup> 5 6 is associated with the stretching vibration of C-N bond in the 2-MIM ligand [32]. The LDH samples are isostructural showing similar peaks. The absorbed peak at 3545 cm<sup>-1</sup> is associated 7 with the OH<sup>-</sup> stretching vibration [33]. It is observed that the band at 1332 cm<sup>-1</sup> appeared in 8 9 LDH samples after the addition of Ni ions, showing that incorporation of Ni ions in MOF alters the environment around the -COO- group. Strong absorption bands at 1317 and 1634 cm<sup>-1</sup> were 10 ascribed to the symmetric and asymmetric stretching vibrations of the coordinated Co-COO-11 Co and Ni-COO-Ni while the peaks at 627, 512, and 420 cm<sup>-1</sup> are for Ni-O and Co-O groups. 12 Compared to NiCo LDH-1, other LDH samples depict sharper peaks, which may be due to 13 abundance of NO<sup>3-</sup> and H<sub>2</sub>O intercalations in LDH interlayers [34]. The XRD diffraction 14 15 patterns of prepared samples depicted in Figure 3(b) show three intense peaks at 44.4°, 51.8°, and 76.4° corresponding to Ni foam. However, a few very weak diffraction peaks as shown in 16 the inset are found at 18°, 21.9°, 26.4°, and 29.6° assigned to the (222), (114), (134), and (044) 17 planes of Co-ZIF, and have been reported by other researchers [35]–[37]. However, these peaks 18 19 were absent in NiCo LDH which may be due to the following two factors, either the Ni foam 20 signal is too intense masking these peaks, or the low mass loading and poor crystallinity of NiCo-LDH samples. The poor crystalline nature of NiCo LDH may be due to the partial 21 substitution of Co<sup>2+</sup> by Ni<sup>2+</sup> ions in the Co-ZIF that distort its initial crystal structure also well 22 23 agreed with the TEM results [33].

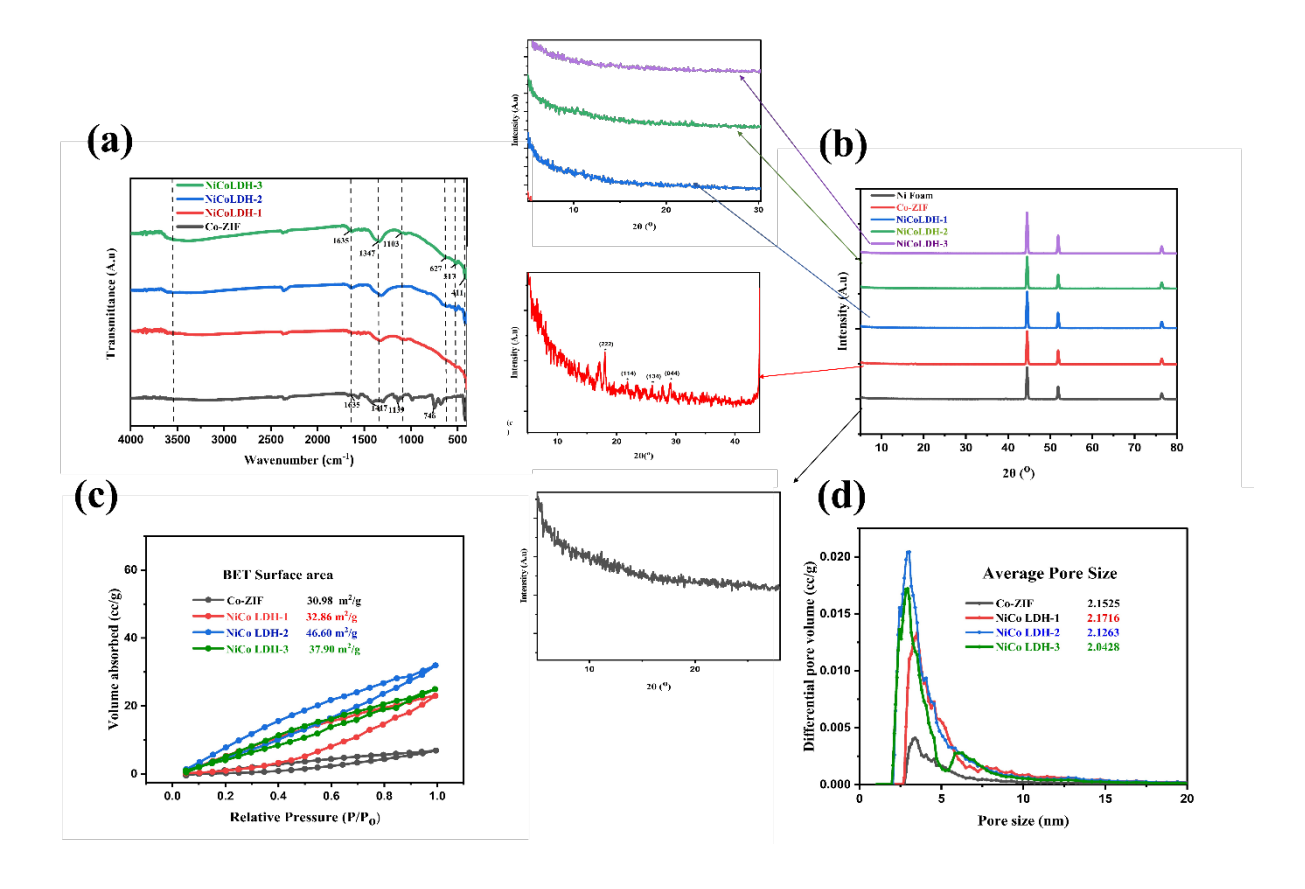


Figure 3: (a) FTIR curve (b) XRD (c, d) BET of as prepared Co-ZIF and Co LDH samples

XPS analysis was used to evaluate the elemental composition and chemical valence states in NiCo LDH-2 sample. The full scan as shown in Figure 4, confirms the existence of cobalt, nickel, oxygen, carbon, and nitrogen elements in the prepared samples. The XPS scan for Co 2p (Figure 4 (b)) displays peaks at 780.9 eV classified for Co 2p<sub>3/2</sub> (Co<sup>2+</sup> at 784.3 and Co<sup>3+</sup> at 781.3 eV) and 796.8 eV classified for Co 2p<sub>1/2</sub> (Co<sup>2+</sup> at 797.3 and Co<sup>3+</sup> at 795.9 eV) attributes to the presence of both Co<sup>3+</sup> and Co<sup>2+</sup>, along with two satellites were present at 786.2 and 802.3 eV. Additionally, the spin-orbit gap of approximately 16.0 eV in the Co 2p graph affirms the generation of the Co(OH)<sub>2</sub> phase. Additionally, XPS scan for Ni 2p (Figure 4 (c)) displays a set of spin–orbit peaks at 852.7 and 870.2 eV attributed to Ni<sup>2+</sup> and another set of peaks at 872.8 and 855 eV allocated to Ni<sup>3+</sup> both sets classified for Ni 2p<sub>1/2</sub> and Ni 2p<sub>3/2</sub> respectively [38]. Two shakeup excitation satellite peaks are also present at 861 and 881.36 eV respectively. The XPS scan for the O 1s (Figure 4 (d)) displays three sharp peaks at 529.7, 531.4, and 532.6

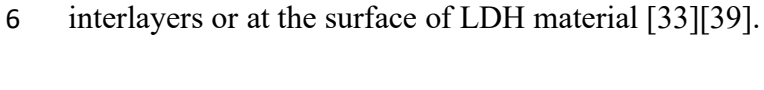
eV classified for hydroxide group (OH<sup>-</sup>), metal (Co, Ni)-oxide bonding, and a hydroxyl group

(H-O-H) confirming the LDH formation[39]. The XPS spectrum for core-level C 1s is

displayed in Figure 4(e). The spectrum shows peaks at 287.0, 285.4, and 284.6 eV classified

for O-C-O, C-O, and C=C groups respectively. They might originate from CO<sub>3</sub><sup>2-</sup> in the LDH

interlayers. The N 1s peak in Figure 4f) at 398.6 eV classifies the existence of nitrate in



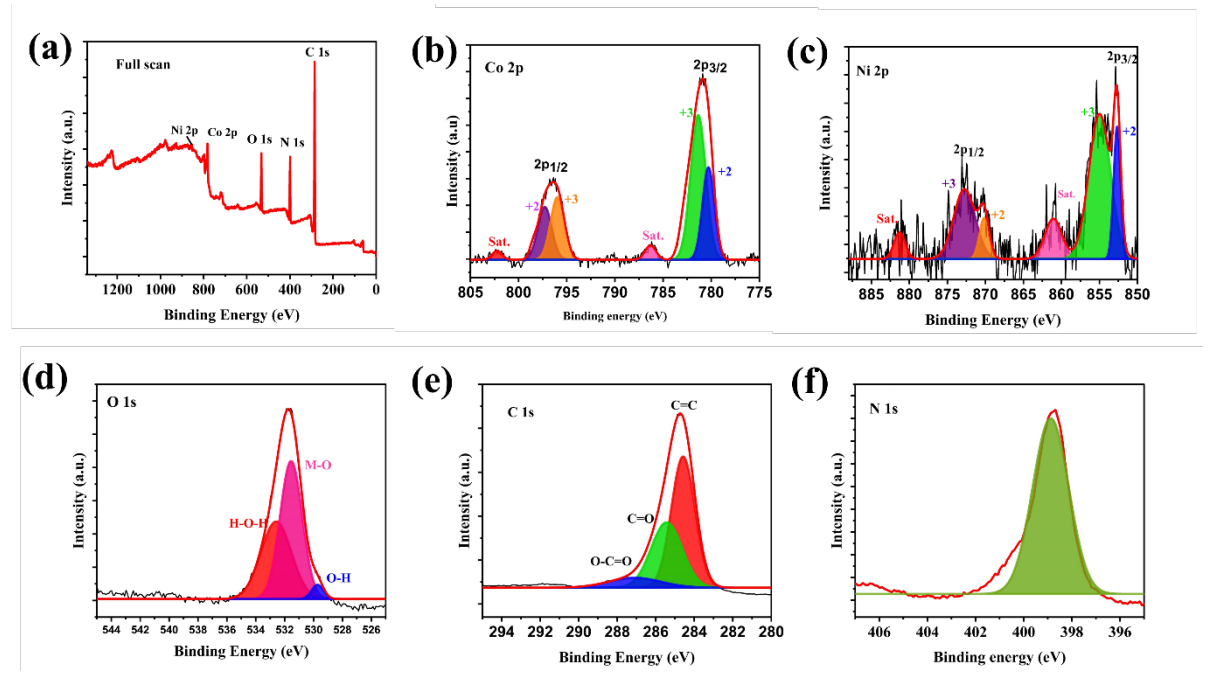


Figure 4: XPS curve (a) Full survey (b) cobalt (c) Nickel (d) Oxygen (e) Carbon (f) Nitrogen for NiCo LDH-2 sample

Further, high specific surface area and optimal pore distribution are essential for the fabrication of efficient charge storage material, BET of Co ZIF and LDH samples were analysed using  $N_2$  adsorption—desorption isotherms [19]. Figure 3(c) illustrates typical IV-type  $N_2$  adsorption—desorption isotherms with hysteresis loop for NiCo-LDHs where a narrow area in the low-pressure region shows an open porous structure whereas, high-pressure region's hysteresis loop suggests the existence of macropores. The BJH curves as illustrated in Figure 3(d), depict a peak centred at around 3 nm that further affirms the mesoporous characteristic of the samples.

- In comparison to other LDH samples and the precursor Co-ZIF, NiCo LDH-2 demonstrated 1
- the highest specific surface area of 46.60 m<sup>2</sup>g<sup>-1</sup> with a total pore volume of 0.0473 ccg<sup>-1</sup>. The 2
- limited specific surface area of LDH materials is generally due to their distinctive structure. 3
- The interlayer spacing of the LDH was partly filled with anions (NO<sub>3</sub>, CO<sub>3</sub>, and OH), ethanol, 4
- and H<sub>2</sub>O molecules, making it challenging to capture the N<sub>2</sub> molecule utilized for the 5
- adsorption-desorption investigation [28]. Yet, during charge/discharge mechanism, the 6
- 7 electrolytic ions can readily penetrate into these interlayer spaces [39]–[41].

#### 3.2. Electrochemical analysis 8

24

Electrochemical properties of binder-free NiCo-LDH electrodes prepared with different Ni 9 concentrations were analysed using a three-electrode configuration (Scheme 2) through CV, 10 11 GCD, and EIS measurements in 1 M KOH electrolytic solution. Figure 5(a) compares the CV 12 of different samples in a potential window of 0.5 V at a scan rate of 5 mVsec<sup>-1</sup>. The hydroxides ions (OH<sup>-</sup>) in the electrolyte promotes the pair of redox peaks visible in the CV curves of LDH 13 samples, implying battery-like behaviour of LDH materials and the specific capacity is given 14 by the reversible redox reactions. However, the specific capacitance LDHs samples initially 15 rises in LDH 1 and 2 and then fall with increasing Ni concentrations. The NiCo LDH-1 offers 16 narrow pathways for electrolyte diffusion due to the porous and interconnected nanosheets. 17 But, because of the low concentration of nickel ions, the electrode was unable to demonstrate 18 improved redox chemistry. Whereas, the dual-layered NiCo LDH-2 sample whose SEM 19 showed slightly widened pathways and firmly adhered star-like nanoarchitectures, boosts 20 redox active sites and serves as an electron highway to reduce the interfacial resistance. 21 Furthermore, the 3D nanostar architecture offers supplemental redox active sites and high 22 electroactive surface area for better energy storage. On the contrary, the NiCo LDH-3 displayed 23 lesser capacity than NiCo LDH-2, which may have been caused by the agglomerated

- 1 nanostructure clusters blocking the ion pathway and also appearance of wider cracks that are
- 2 suboptimal for electrolytic diffusion.

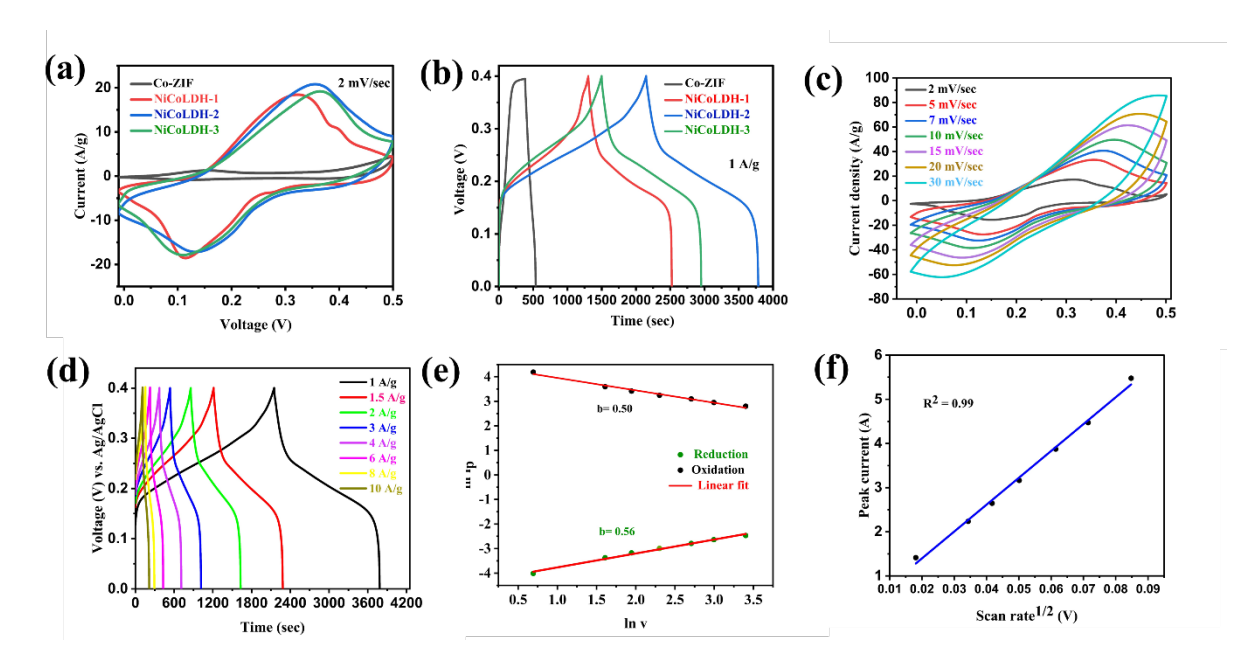


Figure 5: Electrochemical analysis (a) comparative CV (b) GCD curve for Co-ZIF and LDH samples (c) CV (d) GCD for NiCo LDH-2 sample (e) ln i<sub>p</sub> vs ln v (f) i<sub>p</sub> vs V curve for NiCo LDH-2 sample

Higher concentration of Ni may result in extreme etching of the precursor that results in a destructive layered structure in NiCo-LDH-3 sample with wider surface cracks as confirmed by FESEM images in Figure 1(e). This demonstrates that adding an appropriate quantity of Ni can enhance the material's performance, while adding too much negates the effect. The CV curve NiCo LDH-2 shows the largest area offering higher capacitance than other samples which may be attributable to the synergistic effect of Ni and Co and the sample's distinctive structure. Further, the detailed CV curves of sample NiCo LDH-2 from 2 to 30 mVsec<sup>-1</sup> to examine the electrochemical properties are plotted in Figure 5(c). The comparative electrochemical performance with other reported work is compared in Table 1. The redox peaks are derived from the redox reactions of Co<sup>2+</sup>/Co<sup>3+</sup> and Ni<sup>2+</sup>/Ni<sup>3</sup> related to following redox reactions.

$$Co(OH)_2 + OH^- \rightarrow CoOOH + H_2O + e^-$$
....(7)

1 Ni(OH)<sup>2</sup> + OH<sup>-</sup> 
$$\rightarrow$$
 NiOOH + H<sub>2</sub>O + e<sup>-</sup>....(8)  
2 CoOOH + OH<sup>-</sup>  $\rightarrow$  CoO<sub>2</sub> + H<sub>2</sub>O + e<sup>-</sup>....(9)

Table 1: Comparative table for specific capacity of NiCo LDH-2 with other reported work

4	Electrode	Specific	Current	Electrolyte	Potential	Reference
5		capacity (Cg <sup>-1</sup> )	density (Ag <sup>-1</sup> )	(М КОН)	range (V)	
6	CNT@NiCo	579.6	1	6	0-0.5	[29]
7	LDH					
8	CoS <sub>x</sub> /Ni-Co LDH	702.9	1	2	0-0.45	[42]
9	NiCo-LDH/10	1272	2	3	0-0.38	[31]
10	NiCo-	1243.2	1	2	0-0.45	[28]
11	LDH/CFC					
12	NiCo LDH-8	656.95	1	1	0-0.35	[22]
13	NiCo LDH	808.4	1		0-0.55	[43]
	NiCoMn-OH	1153.9	1	1	0-0.55	[38]
14	NiCo LDH	695.75	1	3	0-0.55	[44]
15	NiCo LDH-2	1026	1	1	0-0.4	This work

An increase in scan rate shifts the redox peaks steadily towards higher potential increases the peak current height owing to high polarization, OH<sup>-</sup> diffusion and internal resistance. However, there is no discernible change in the shape of the curves, demonstrating good reversibility and also rapid ion mass transfer of the electrode. Furthermore, the CV curves are also investigated to analyse the electrochemical reaction kinetics of the electrode using Dunn's power law formula given below:

23 
$$i = kv^b$$
.....(10)

24 
$$\ln(i) = \ln(k) + b \ln(v)$$
....(11)

Where i defines current density (Ag<sup>-1</sup>), v (mVsec<sup>-1</sup>) is scan speed, and k and b are adjustable 1 parameters, where b is an important parameter related to the charge storage mechanism. 2 Ideally, b is found to be 1 for EDLC supercapacitors and capacitors, where charge storage is 3 mainly through the electrostatic mechanism. In the case of batteries value of b is found to be 4 0.5, as charge storage is through a faradic mechanism (oxidation-reduction). Figure 5(e) shows 5 a linear relation between ln ip and ln v. The b values are 0.50 and 0.56 for anodic and cathodic 6 7 peaks respectively that is less than 1 and near 0.5. As a result, both the surface-controlled and diffusion-controlled processes operate simultaneously on NiCo LDH-2, with the diffusion-8 9 controlled process predominating during the charge storage mechanism. Further, the plot of peak current with scan rate illustrated in Figure 5(f), demonstrates excellent linearity (R<sup>2</sup> = 10 0.99) signifying deep OH- ion penetration in NiCo LDH-2, through superior diffusion-11 controlled charge storage technique. 12 GCD tests are also performed to analyse the electrochemical behaviour of samples with the 13 potential window of 0.0-0.4 V. Figure 5(b) shows the comparative curve for different samples 14 at a current density of 1 Ag-1. All of LDH electrodes demonstrate longer discharge time as 15 compared to Co-ZIF electrode. Particularly, the NiCo LDH-2 showed the highest discharge 16 time amongst all electrodes in concurrence with the CV results. NiCo LDH-2 has adequate 17 amount of oxidation/reduction sites and a distinct network-like structure, which promotes the 18 intercalation of ions in interlayers of LDH, resulting in remarkable specific capacitance which 19 makes it a promising positive electrode for the fabrication of supercapattery device. The 20 specific capacity for sample NiCo LDH-2 is found to be 1026 Cg<sup>-1</sup> (2567 Fg<sup>-1</sup>) which is higher 21 than that of NiCo LDH-1, NiCo LDH-3, and Co-ZIF that is 760.4 Cg<sup>-1</sup>, 907.2 Cg<sup>-1</sup>, and 54.4 22 Cg<sup>-1</sup> respectively at a current density of 1 Ag<sup>-1</sup>. The detailed GCD curve for sample NiCo LDH-23 2 from 1 to 10 Ag<sup>-1</sup> as shown in Figure 5(d) shows a drop-off in the specific capacity with 24 increasing current density. This may be due to a gradual transition of redox mechanism to 25

- surface-controlled, which eventually results in attenuation of the specific capacity [39]. The
- 2 obvious redox plateaus are maintained in the discharge curve even at high current density, the
- 3 sample NiCo LDH-2 could reach a level of 637.2 Cg<sup>-1</sup> even at the current density of 10 Ag<sup>-1</sup>,
- 4 indicating fast electron transfer kinetics in the electrode.
- 5 To evaluate the information regarding the ion diffusion and electron transfer kinetics at the
- 6 electrode-electrolyte interface, EIS analysis was carried out in 100 kHz to 0.01 Hz frequency
- 7 range. Figure 6a) illustrates the comparative Nyquist curve. The Nyquist plot typically consists
- 8 of two regions: a straight line at the low frequency and a semicircle arc at the high-frequency
- 9 region. Series resistance (Rs), consists of the interfacial resistance between the electrode and
- the current collector as well as the series resistance of the electrode materials, electrolyte, and
- current collectors determined by calculating the intercept of the origin of the semi-circle arc
- with real impedance (Z') axis. It was observed that lower R<sub>s</sub> (1.45 Ohm) was found in NiCo
- LDH-2 than NiCo LDH-1 (1.84 Ohm) and NiCo LDH-3 (2.13 Ohm), indicating faster electron
- transport, improved conductivity, improved electron transfer kinetics, and electrochemical
- activity in NiCo LDH-2 samples, well supported the CV and GCD results. The semicircle at
- high frequency corresponds to the charge transfer resistance (R<sub>ct</sub>) resulted from the faradic
- 17 reactions at the electrode interface. R<sub>ct</sub> is strongly influenced by the conductivity of the
- electrode materials. The R<sub>ct</sub> value for Co-ZIF, NiCo LDH-1, 2, 3 was found to be 0.2999, 0.91,
- 19 0.1 and 0.99 Ohm respectively. A notably straight line at the low-frequency region refers to
- 20 enhanced capacitive performance with unrestricted ion diffusion. Nyquist plot of NiCo LDH-
- 21 2 indicates a notably vertical line, demonstrating high capacitive nature, and faster ion diffusion
- speed compared to Co-ZIF and other LDH electrodes [39][45].

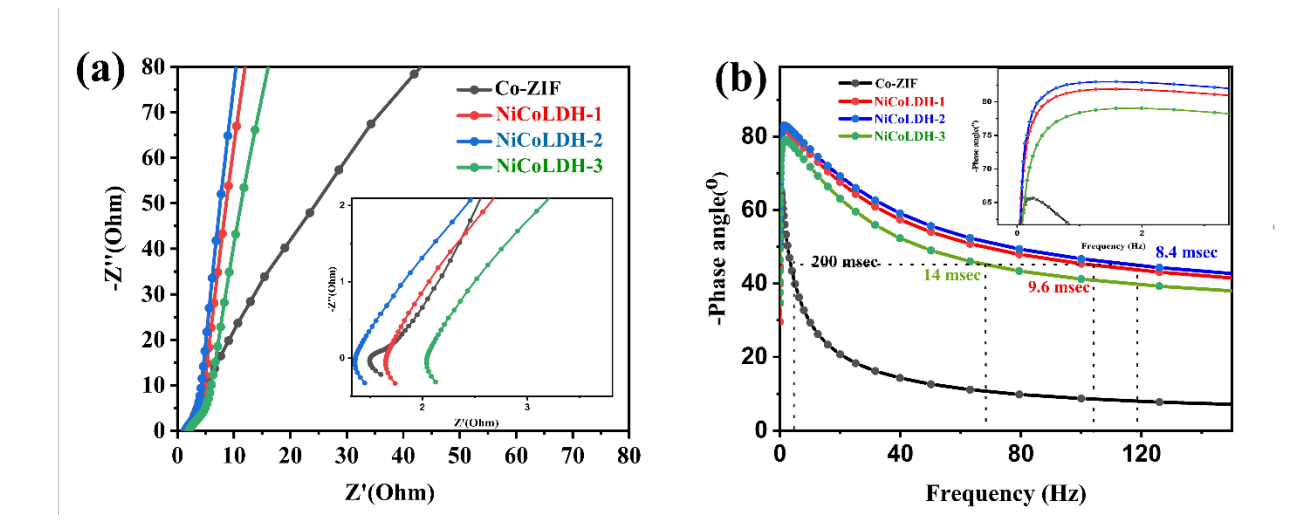


Figure 6: Electrochemical analysis (a) comparative Nyquist (b) Bode plot for Co-ZIF and other

NiCo LDH sample

Bode plots were used to explore the ion diffusion kinetics as shown in Figure 6(b) and can be

evaluated by the equation  $\tau_o = 1/f_o$ , where  $\tau_o$  is the relaxation constant and  $f_o$  is the frequency at the phase angle of  $-45^o$  [46]. The relaxation constant of Co-ZIF, NiCo LDH-1, 2, 3 electrodes was found to be 200 msec, 9.6 msec, 8.4 msec, and 14 msec. Lower relaxation constant of the NiCo LDH-2 electrode indicates a fast ion diffusion process and high power of the electrode [45]. Based on the aforementioned analyses, it can be concluded that distinctive porous structure of NiCo-LDH-2 with good intrinsic conductivity accelerates ion transfer during redox reactions, leading to remarkable electrochemical performance.

The value obtained for NiCo LDH-2 electrode demonstrates that the material is capable of delivering its stored energy in faster time scale with high power. In addition, the porous network surface of NiCo LDH-2 provides ample active sites that boosts specific capacitance and other electrochemical parameters, making it a potential electrode material for highly efficient supercapattery.

# 4. Electrochemical properties of the supercapattery device assembled by sample NiCo LDH-2 and coffee grounds derived rGO

- 1 For practical applications, a supercapattery device was fabricated using NiCo LDH-2 as an
- 2 anode and rGO as cathode in 1 M KOH electrolytic solution. The as-prepared rGO shows
- 3 nearly rectangular-shaped CV curves (Figure 7(a)) and symmetrical GCD curves (Figure 7(b))
- 4 suggesting that rGO is a typical electric double-layer capacitive material.

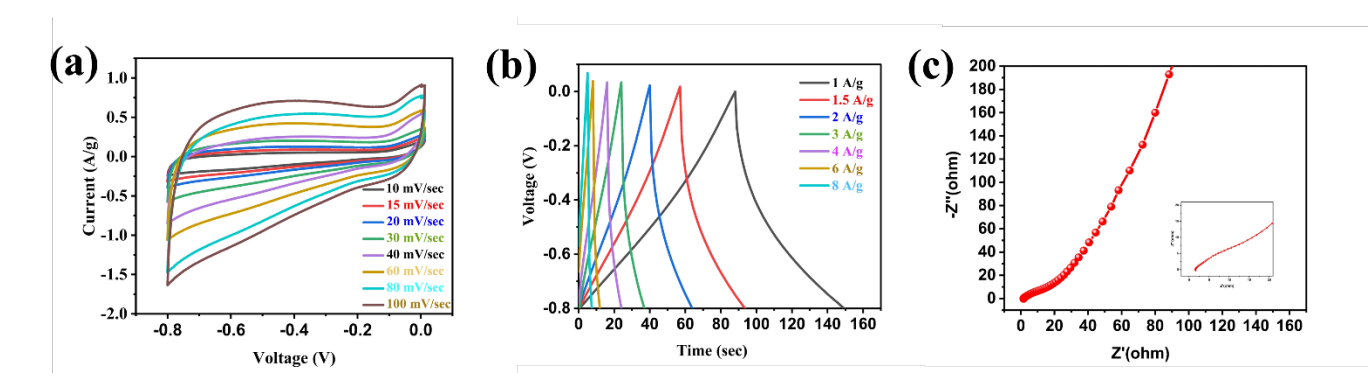


Figure 7: Electrochemical analysis for coffee grounds derived rGO (a) CV (b) GCD (c) EIS

The CV curves of NiCo LDH-2 and rGO at a scan rate of 15 mVsec<sup>-1</sup> are shown in Figure 8(b). The curve shows that the potential range of the rGO electrode is stable from -0.8 to 0 V, while the potential range of NiCo LDH-2 is stable from 0 to 0.4 V. Therefore, the operating voltage of NiCo LDH-2//rGO can be extended to 1.2 V [47]. The optimum mass ratio of anode to cathode was found to be 1:9.66, using the mass balancing equation (6). The quasi-rectangular-shaped CV curves show that the total capacitance of the supercapattery device collectively accounts for the electric double layer capacitance (EDLC) and the pseudocapacitance (Figure 8(c)). Furthermore, as the scan rate increases, no discernible curve shape deformation was observed in the CV, indicating the device's high reversibility and great functioning, which is further validated by the GCD curve (Figure 8(d)).

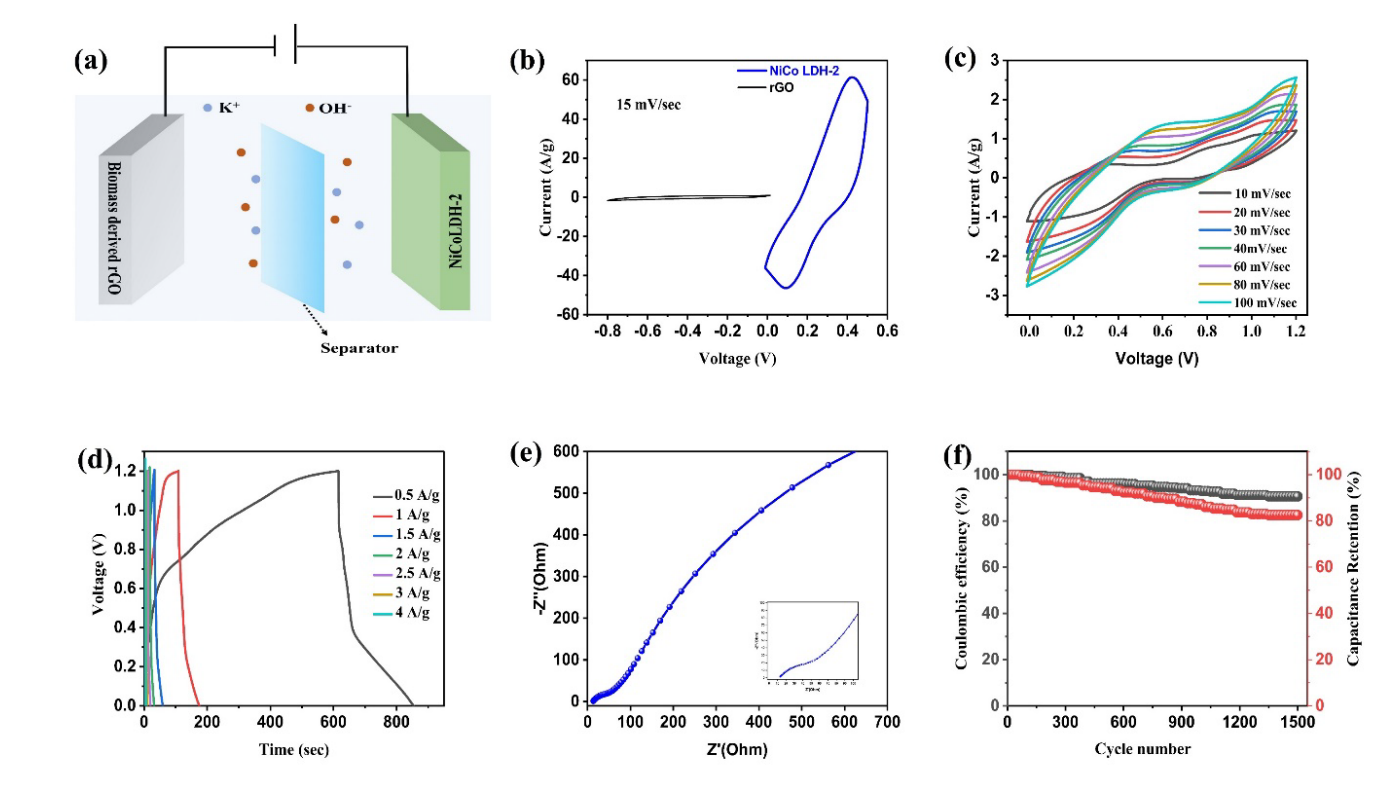


Figure 8: Electrochemical analysis for NiCo LDH-2//rGO supercapattery device (a) assembly (b) comparative CV curve for NiCo LDH-2 and rGO at 15 mVsec<sup>-1</sup> (c) CV (d) GCD (e) EIS (f) cyclic performance

The EIS spectrum (Figure 8) of the device displays R<sub>s</sub> of 12 Ω and R<sub>ct</sub> of 38 Ω, demonstrating efficient charge transfer and good conductivity. Further, the specific capacitance, energy density, and power density of the supercapattery device can be calculated using equations (3-5). The specific capacitance of the supercapattery device is found to be 102.5 Fg<sup>-1</sup> at the current density of 0.5 Ag<sup>-1</sup> [29]. The NiCo-LDH//rGO device reveals a higher energy density of 21 Whkg<sup>-1</sup> at a power density of 0.307 kWkg<sup>-1</sup> at an operating voltage of 1.2 V, surpassing some of the previously reported supercapattery devices Zn-NiHCF//solar carbon (9.1 Whkg<sup>-1</sup>, 0.153 kWkg<sup>-1</sup>) [48], Mn-CoS-3//AC (17.94 Whkg<sup>-1</sup> at 806 Wkg<sup>-1</sup>) [49], Bi<sub>2</sub>O<sub>3</sub>//graphite (8 Whkg<sup>-1</sup>, 2040 Wkg<sup>-1</sup>) [50], NiS<sub>2</sub>@NiV<sub>2</sub>S<sub>4</sub>//AC (19.4 Whkg<sup>-1</sup>, 140 Wkg<sup>-1</sup>) [50], MXene/NiS//AC (17.68 Whkg<sup>-1</sup>, 750 Wkg<sup>-1</sup>) [51], AC//Li<sub>2</sub>MnSiO<sub>4</sub>/Al<sub>2</sub>O<sub>3</sub> (17.688 Whkg<sup>-1</sup>, 407.2 Wkg<sup>-1</sup>) [52]. The cycling performance (Figure 8(f)) of the NiCo-LDH-2//rGO device at 3 Ag<sup>-1</sup> is shown in Figure

8(f) after 1500 repeated charge-discharge cycles, the device exhibits high capacitance retention of 88.89 % with coulombic efficiency of 90.58 %. Further, SEM and XRD studies on NiCo LDH-2 after 1500 cycles were done to investigate the change in morphology and crystallinity of the sample. The XRD pattern of the LDH electrode post cyclability test (Figure S4) showed no additional peaks apart from peaks corresponding to Ni foam substrate. The SEM image of the post cyclability test sample (Figure 9) shows a similar porous structure as the pristine sample (Figure 1d) with moderate changes in the morphology showing a marginal breakdown in the 3D structure of LDH during extended cycling. Further, the EDX pattern of pre and post cyclability test sample have been depicted in Figure S5 (a, b), showing emergence of a new peak corresponding to potassium due to partial electrolyte absorption on the NiCo LDH electrode. Given its remarkable electrochemical performance, the hybrid supercapattery system holds significant promise as a prospective device in the realm of energy storage systems.

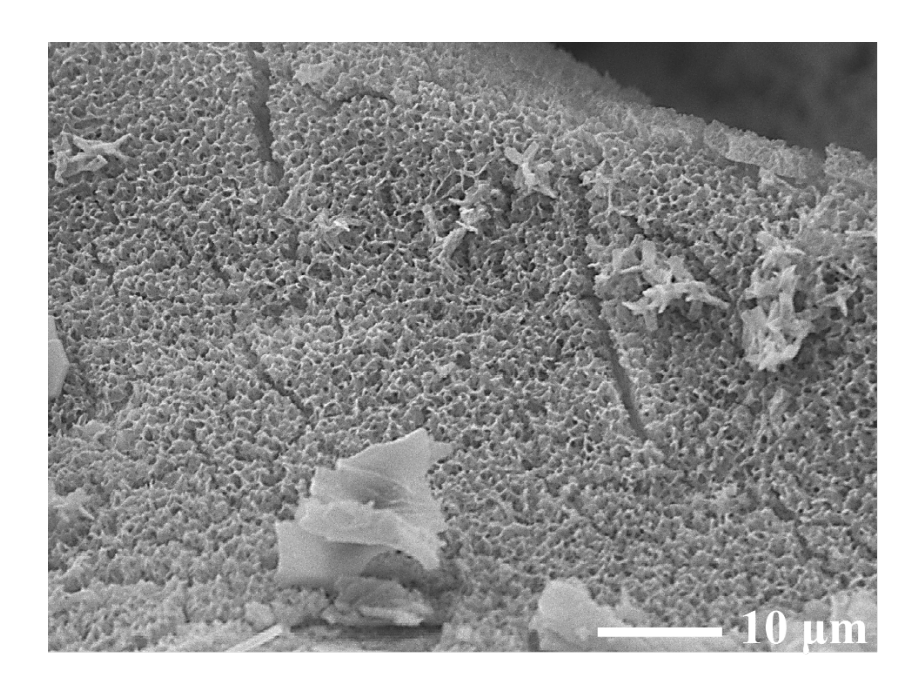


Figure 9: SEM image of NiCo LDH-2 after cyclability test

This study presents an easy design strategy to architect multifaceted metal hydroxide with welldefined inner voids composed of biomass precursor for highly efficient electrochemical

applications. It is important to note that by tailoring the experimental parameters, such as improving the contact between the electrolyte and electrodes and optimising the loading of rGO to match the capacitance of the NiCo LDH material, the performance of the supercapattery device may be further enhanced. Not only does the current work involves formation of highly efficient NiCo LDH electrode suitable for supercapattery applications, but also key sustainability benefits. This approach leverages recovery of bio resources to produce reduced graphene oxide (rGO) from coffee grounds through microwave pyrolysis and subsequent treatments. The promising results demonstrated by NiCo LDH//rGO based supercapattery device and further innovative research along with material engineering may lead to development of advanced strategic functionality suitable for high performance handheld electronic devices. 

#### 5. Conclusion

In summary, we have adopted a novel technique to synthesized NiCo-LDH derived from Co-ZIF as a precursor directly on Ni foam via ion exchange method. In the process, concentration of Ni is optimised to maintain sturdiness of the porous structure and allowing greatest possible interaction between transition metals that offer strong synergy and rapid redox reactions with notable electrical conductivity. We identified that NiCo LDH material has excellent potential for the preparation of binder-free supercapattery electrodes. Benefiting from the distinctive structure, the prepared NiCo LDH electrode exhibits a remarkable specific capacitance of 2567 Fg<sup>-1</sup> (1026 Cg<sup>-1</sup>) at 1 Ag<sup>-1</sup> which is much higher than the Co-ZIF precursor. Further, for the practical applications, coffee grounds-derived rGO was used as cathode. The NiCo LDH-2//rGO supercapattery device delivers specific capacitance (102.5 Fg<sup>-1</sup> at 0.5 Ag<sup>-1</sup>), energy density (21 Whkg<sup>-1</sup> at 0.307 kWkg<sup>-1</sup>) and good cycling life (maintaining capacitance retention of 88.89 % with coulombic efficiency of 90.58 % over 1500 cycles). Further, this work may

- offer an innovative approach for designing and fabricating new porous LDH materials, which
- 2 could be used for prospective high-performance energy storage applications.

#### 3 Acknowledgement

- 4 Author Megha Prajapati is thankful for the financial support provided by IGDTUW, Delhi for
- 5 research work. The authors thanks Dr. Akhilesh Pandey (Scientist F), Solid State Physics
- 6 Laboratory, Defence Research and Development Organisation, India for helping in XRD
- 7 investigations.

8

9

10

#### Reference

- 11 [1] T. Kim, W. Song, D. Y. Son, L. K. Ono, and Y. Qi, "Lithium-ion batteries: outlook on present, future, and hybridized technologies," *J. Mater. Chem. A*, vol. 7, no. 7, pp.
- 13 2942–2964, 2019, doi: 10.1039/C8TA10513H.
- 14 [2] S. Ma *et al.*, "Temperature effect and thermal impact in lithium-ion batteries: A review," *Prog. Nat. Sci. Mater. Int.*, vol. 28, no. 6, pp. 653–666, 2018, doi:
- 16 10.1016/j.pnsc.2018.11.002.
- 17 [3] H. Zhang, C. Mao, J. Li, and R. Chen, "Advances in electrode materials for Li-based rechargeable batteries," *RSC Adv.*, vol. 7, no. 54, pp. 33789–33811, 2017, doi: 10.1039/c7ra04370h.
- 20 [4] S. Saffirio, M. Falco, G. B. Appetecchi, F. Smeacetto, and C. Gerbaldi,
- 21 "Li1.4Al0.4Ge0.4Ti1.4(PO4)3 promising NASICON-structured glass-ceramic
- 22 electrolyte for all-solid-state Li-based batteries: Unravelling the effect of diboron
- 23 trioxide," *J. Eur. Ceram. Soc.*, vol. 42, no. 3, pp. 1023–1032, 2022, doi:
- 24 10.1016/j.jeurceramsoc.2021.11.014.
- J. Xie, P. Yang, Y. Wang, T. Qi, Y. Lei, and C. M. Li, "Puzzles and confusions in supercapacitor and battery: Theory and solutions," *J. Power Sources*, vol. 401, no.
- 27 September, pp. 213–223, 2018, doi: 10.1016/j.jpowsour.2018.08.090.
- Y. Zhang *et al.*, "Recent advances and challenges of electrode materials for flexible supercapacitors," *Coord. Chem. Rev.*, vol. 438, p. 213910, 2021, doi:
- 30 10.1016/j.ccr.2021.213910.
- 31 [7] S. H. Nagarajarao et al., "Recent Developments in Supercapacitor Electrodes: A Mini
- Review," *ChemEngineering*, vol. 6, no. 1, p. 5, 2022, doi:
- 33 10.3390/chemengineering6010005.
- 34 [8] C. Shi, J. Sun, Y. Pang, Y. P. Liu, B. Huang, and B. T. Liu, "A new potassium dual-
- ion hybrid supercapacitor based on battery-type Ni(OH)2 nanotube arrays and

- pseudocapacitor-type V2O5-anchored carbon nanotubes electrodes," *J. Colloid Interface Sci.*, vol. 607, pp. 462–469, 2022, doi: 10.1016/j.jcis.2021.09.011.
- M. Z. Iqbal and U. Aziz, "Supercapattery: Merging of battery-supercapacitor electrodes for hybrid energy storage devices," *J. Energy Storage*, vol. 46, no. November 2021, p. 103823, 2022, doi: 10.1016/j.est.2021.103823.
- 6 [10] A. Das, B. Raj, M. Mohapatra, S. M. Andersen, and S. Basu, "Performance and future directions of transition metal sulfide-based electrode materials towards supercapacitor/supercapattery," *Wiley Interdiscip. Rev. Energy Environ.*, vol. 11, no. 1, 2022, doi: 10.1002/wene.414.
- 10 [11] L. Yu and G. Zheng, "Supercapatteries as High Performance Electrochemical Energy 11 Storage Devices," *Electrochem. Energy Rev.*, vol. 3, no. 2, pp. 271–285, 2020, doi: 12 10.1007/s41918-020-00063-6.
- 13 [12] R. Kumari, S. Kumar Sharma, V. Singh, and C. Ravi Kant, "Facile, two-step synthesis of activated carbon soot from used soybean oil and waste engine oil for supercapacitor electrodes," *Mater. Today Proc.*, vol. 67, no. xxxx, pp. 483–489, 2022, doi: 10.1016/j.matpr.2022.07.253.
- 17 [13] S. Gupta, C. Ravikant, and A. Kaur, "One-pot wet chemical synthesis of reduced graphene oxide-zinc oxide nanocomposites for fast and selective ammonia sensing at room temperature," *Sensors Actuators, A Phys.*, vol. 331, p. 112965, 2021, doi: 10.1016/j.sna.2021.112965.
- 21 [14] R. Goel, R. Jha, and C. Ravikant, "Synergistic effect of Urea and Potassium Sulphate during hydrothermal synthesis of NiO nanospheres with reduced crystallite size and enhanced electrical conductivity," *Inorg. Chem. Commun.*, vol. 141, no. February, p. 109563, 2022, doi: 10.1016/j.inoche.2022.109563.
- 25 [15] R. Goel, R. Jha, and C. Ravikant, "Investigating the structural, electrochemical, and optical properties of p-type spherical nickel oxide (NiO) nanoparticles," *J. Phys. Chem. Solids*, vol. 144, no. November 2019, p. 109488, 2020, doi: 10.1016/j.jpcs.2020.109488.
- 29 [16] R. Chaudhari, A. Garg, K. Singh, M. Tomar, V. Gupta, and C. RaviKant, "Bismuth tri30 iodide-polystyrene composite for X-rays switching applications at room temperature,"
  31 *Radiat. Phys. Chem.*, vol. 186, no. April, p. 109538, 2021, doi:
  32 10.1016/j.radphyschem.2021.109538.
- R. Chaudhari and C. RaviKant, "A review on BiI3 perovskites and composites for direct X-ray detection," *Sensors Actuators A Phys.*, vol. 346, no. August, p. 113863, 2022, doi: 10.1016/j.sna.2022.113863.
- P. R. Kharangarh, N. M. Ravindra, G. Singh, and S. Umapathy, "Synthesis and characterization of Nb-doped strontium cobaltite@GQD electrodes for high performance supercapacitors," *J. Energy Storage*, vol. 55, no. PA, p. 105388, 2022, doi: 10.1016/j.est.2022.105388.
- 40 [19] R. Kumari, V. Singh, and C. Ravi, "Enhanced performance of activated carbon-based supercapacitor derived from waste soybean oil with coffee ground additives," *Mater. Chem. Phys.*, vol. 305, no. February, p. 127882, 2023, doi: 10.1016/j.matchemphys.2023.127882.

- B. Akinwolemiwa and G. Z. Chen, "Fundamental consideration for electrochemical engineering of supercapattery," *J. Braz. Chem. Soc.*, vol. 29, no. 5, pp. 960–972, 2018, doi: 10.21577/0103-5053.20180010.
- [21] S. Balasubramaniam, A. Mohanty, S. K. Balasingam, S. J. Kim, and A. Ramadoss,
   Comprehensive Insight into the Mechanism, Material Selection and Performance
   Evaluation of Supercapatteries, vol. 12, no. 1. Springer Singapore, 2020. doi:
   10.1007/s40820-020-0413-7.
- M. U. Tahir *et al.*, "Room temperature and aqueous synthesis of bimetallic ZIF derived CoNi layered double hydroxides and their applications in asymmetric supercapacitors," *J. Colloid Interface Sci.*, vol. 579, pp. 195–204, 2020, doi: 10.1016/j.jcis.2020.06.050.
- 12 [23] X. Li, D. Du, Y. Zhang, W. Xing, Q. Xue, and Z. Yan, "Layered double hydroxides toward high-performance supercapacitors," *J. Mater. Chem. A*, vol. 5, no. 30, pp. 15460–15485, 2017, doi: 10.1039/c7ta04001f.
- [24] S. Sundriyal, H. Kaur, S. K. Bhardwaj, S. Mishra, K. H. Kim, and A. Deep, "Metalorganic frameworks and their composites as efficient electrodes for supercapacitor applications," *Coord. Chem. Rev.*, vol. 369, pp. 15–38, 2018, doi: 10.1016/j.ccr.2018.04.018.
- F. Boorboor Ajdari *et al.*, "A review on the field patents and recent developments over the application of metal organic frameworks (MOFs) in supercapacitors," *Coord. Chem. Rev.*, vol. 422, p. 213441, 2020, doi: 10.1016/j.ccr.2020.213441.
- [26] D. Sheberla, J. C. Bachman, J. S. Elias, C. J. Sun, Y. Shao-Horn, and M. Dincă,
   "Conductive MOF electrodes for stable supercapacitors with high areal capacitance,"
   Nat. Mater., vol. 16, no. 2, pp. 220–224, 2017, doi: 10.1038/nmat4766.
- [27] M. Prajapati, V. Singh, M. V. Jacob, and C. Ravi Kant, "Recent advancement in metalorganic frameworks and composites for high-performance supercapatteries," *Renew. Sustain. Energy Rev.*, vol. 183, no. June, p. 113509, 2023, doi: 10.1016/j.rser.2023.113509.
- T. Wang *et al.*, "2-Methylimidazole-Derived Ni-Co Layered Double Hydroxide Nanosheets as High Rate Capability and High Energy Density Storage Material in Hybrid Supercapacitors," *ACS Appl. Mater. Interfaces*, vol. 9, no. 18, pp. 15510– 15524, 2017, doi: 10.1021/acsami.7b02987.
- H. Niu, Y. Zhang, Y. Liu, N. Xin, and W. Shi, "NiCo-layered double-hydroxide and carbon nanosheets microarray derived from MOFs for high performance hybrid supercapacitors," *J. Colloid Interface Sci.*, vol. 539, pp. 545–552, 2019, doi: 10.1016/j.jcis.2018.12.095.
- [30] G. Nagaraju, S. C. Sekhar, B. Ramulu, S. K. Hussain, D. Narsimulu, and J. S. Yu,
   "Ternary MOF-Based Redox Active Sites Enabled 3D-on-2D Nanoarchitectured
   Battery-Type Electrodes for High-Energy-Density Supercapatteries," *Nano-Micro Lett.*, vol. 13, no. 1, pp. 1–18, 2021, doi: 10.1007/s40820-020-00528-9.
- R. Ramachandran, Y. Lan, Z. X. Xu, and F. Wang, "Construction of NiCo-Layered Double Hydroxide Microspheres from Ni-MOFs for High-Performance Asymmetric Supercapacitors," *ACS Appl. Energy Mater.*, vol. 3, no. 7, pp. 6633–6643, 2020, doi: 10.1021/acsaem.0c00790.

- 1 [32] H. Guo, Y. Wang, C. Li, and K. Zhou, "Construction of sandwich-structured CoAllayered double hydroxide@zeolitic imidazolate framework-67 (CoAl-LDH@ZIF-67) hybrids: Towards enhancing the fire safety of epoxy resins," *RSC Adv.*, vol. 8, no. 63, pp. 36114–36122, 2018, doi: 10.1039/c8ra06355a.
- 5 [33] S. Gao *et al.*, "Dandelion-like nickel/cobalt metal-organic framework based electrode materials for high performance supercapacitors," *J. Colloid Interface Sci.*, vol. 531, pp. 83–90, 2018, doi: 10.1016/j.jcis.2018.07.044.
- T. K. Ghosh, D. L. Singh, V. Mishra, M. K. Sahoo, and G. R. Rao, "Synthesis of Nico-Ldh Using Zif-67 Nanoflake Precursor in Combination with Reduced Graphene Oxide (Rgo) for High Performance Supercapattery Application," *SSRN Electron. J.*, vol. 1, pp. 1–39, 2022, doi: 10.2139/ssrn.4039688.
- 12 [35] N. M. Umesh, J. Antolin Jesila, S. F. Wang, N. Vishnu, and Y. J. Yang, "Novel voltammetric detection of norfloxacin in urine and blood serum using a flexible Ni foam based Ni-Co-MOF ultrathin nanosheets derived from Ni-Co-LDH," *Microchem.* J., vol. 160, no. PB, p. 105747, 2021, doi: 10.1016/j.microc.2020.105747.
- [36] Z. Yang *et al.*, "Construction of 2D ZIF-derived hierarchical and hollow NiCo-LDH nanosheet-on-nanosheet' arrays on reduced graphene oxide/Ni foam for boosted electrochemical energy storage," *J. Alloys Compd.*, vol. 850, p. 156864, 2021, doi: 10.1016/j.jallcom.2020.156864.
- 20 [37] A. Tang, P. Chen, and C. Mi, "Ni-Co layered double hydroxide nanosheet array on nickel foam coated graphene for high-performance asymmetric supercapacitors,"
  22 Ionics (Kiel)., vol. 26, no. 12, pp. 6277–6287, 2020, doi: 10.1007/s11581-020-0372923 9.
- 24 [38] C. Kang *et al.*, "Metal-organic framework derived hollow rod-like NiCoMn ternary metal sulfide for high-performance asymmetric supercapacitors," *Chem. Eng. J.*, vol. 427, no. June 2021, p. 131003, 2022, doi: 10.1016/j.cej.2021.131003.
- H. Wang, Q. He, F. Zhan, and L. Chen, "Fe, Co-codoped layered double hydroxide nanosheet arrays derived from zeolitic imidazolate frameworks for high-performance aqueous hybrid supercapacitors and Zn-Ni batteries," *J. Colloid Interface Sci.*, vol. 630, pp. 286–296, 2023, doi: 10.1016/j.jcis.2022.09.092.
- C. Liu, Y. Bai, J. Wang, Z. Qiu, and H. Pang, "Controllable synthesis of ultrathin layered transition metal hydroxide/zeolitic imidazolate framework-67 hybrid nanosheets for high-performance supercapacitors," *J. Mater. Chem. A*, vol. 9, no. 18, pp. 11201–11209, 2021, doi: 10.1039/d1ta02065j.
- J. J. Zhou *et al.*, "Controllable transformation of CoNi-MOF-74 on Ni foam into hierarchical-porous Co(OH)2/Ni(OH)2 micro-rods with ultra-high specific surface area for energy storage," *Chem. Eng. J.*, vol. 428, no. August 2021, pp. 1–9, 2022, doi: 10.1016/j.cej.2021.132123.
- X. Guan, M. Huang, L. Yang, G. Wang, and X. Guan, "Facial design and synthesis of CoSx/Ni-Co LDH nanocages with rhombic dodecahedral structure for high-performance asymmetric supercapacitors," *Chem. Eng. J.*, vol. 372, no. January, pp. 151–162, 2019, doi: 10.1016/j.cej.2019.04.145.
- L. Hou *et al.*, "Ni-Co layered double hydroxide with self-assembled urchin like morphology for asymmetric supercapacitors," *Mater. Lett.*, vol. 237, pp. 262–265,

- 1 2019, doi: 10.1016/j.matlet.2018.11.123.
- F. Cao *et al.*, "Hierarchical sheet-like Ni–Co layered double hydroxide derived from a MOF template for high-performance supercapacitors," *Synth. Met.*, vol. 234, no. November, pp. 154–160, 2017, doi: 10.1016/j.synthmet.2017.11.001.
- 5 [45] M. G. Radhika *et al.*, "Electrochemical studies on Ni, Co & Ni/Co-MOFs for high-6 performance hybrid supercapacitors," *Mater. Res. Express*, vol. 7, no. 5, 2020, doi: 10.1088/2053-1591/ab8d5d.
- [46] L. Gurusamy *et al.*, "Enhanced performance of charge storage supercapattery by dominant oxygen deficiency in crystal defects of 2-D MoO3-x nanoplates," *Appl. Surf.* Sci., vol. 541, no. November 2020, p. 148676, 2021, doi: 10.1016/j.apsusc.2020.148676.
- 12 [47] B. Zhang, S. Song, W. Li, L. Zheng, and X. Ma, "Asymmetric supercapacitors with high energy density and high specific capacitance based on Ni-Co-Mn multiphase metal structure MOF," *Ionics (Kiel)*., vol. 27, no. 8, pp. 3553–3566, 2021, doi: 10.1007/s11581-021-04056-3.
- D. R. Lobato-peralta, J. Vazquez-samperio, O. Pérez, P. Acevedo-peña, E. Reguera, and A. K. Cuentas-gallegos, "Potassium-ion aqueous supercapattery composed by solar carbon and nickel- zinc prussian blue analogue," *J. Energy Storage*, vol. 31, no. April, p. 101667, 2020, doi: 10.1016/j.est.2020.101667.
- 20 [49] G. Surender, F. S. Omar, S. Bashir, M. Pershaanaa, S. Ramesh, and K. Ramesh, "Growth of nanostructured cobalt sulfide-based nanocomposite as faradaic binder-free electrode for supercapattery," *J. Energy Storage*, vol. 39, no. October 2020, p. 102599, 2021, doi: 10.1016/j.est.2021.102599.
- 24 [50] N. M. Shinde *et al.*, "Ultra-rapid chemical synthesis of mesoporous Bi2O3 microsponge-balls for supercapattery applications," *Electrochim. Acta*, vol. 296, pp. 308–316, 2019, doi: 10.1016/j.electacta.2018.11.044.
- 27 [51] H. Liu *et al.*, "A facile method for synthesizing NiS nanoflower grown on MXene (Ti3C2Tx) as positive electrodes for 'supercapattery," *Electrochim. Acta*, vol. 353, p. 136526, 2020, doi: 10.1016/j.electacta.2020.136526.
- M. M. Ndipingwi *et al.*, "Orthorhombic Nanostructured Li2MnSiO4/Al2O3
   Supercapattery Electrode with Efficient Lithium-Ion Migratory Pathway," *Batter.* Supercaps, vol. 1, no. 6, pp. 223–235, 2018, doi: 10.1002/batt.201800045.